Journal of Power Sources 330 (2016) 120–126

Contents lists available at ScienceDirect

Journal of Power Sources

journal homepage: www.elsevier.com/locate/jpowsour

All-solid-state lithium–sulfur batteries with three-dimensional mesoporous electrode structures

Miki Nagao [a], Kota Suzuki [a, b], Yuki Imade [a], Mitsuru Tateishi [a], Ryota Watanabe [c], Toshiyuki Yokoi [c, d], Masaaki Hirayama [a, b], Takashi Tatsumi [c], Ryoji Kanno [a, b, *]

[a] Department of Electronic Chemistry, Interdisciplinary Graduate School of Science and Engineering, Tokyo Institute of Technology, Yokohama 226-8502, Japan
[b] Department of Chemical Science and Engineering, School of Materials and Chemical Technology, Tokyo Institute of Technology, Yokohama 226-8502, Japan
[c] Chemical Resources Laboratory, Tokyo Institute of Technology, Yokohama 226-8503, Japan
[d] Laboratory for Chemistry and Life Science, Institute of Innovative Research, Tokyo Institute of Technology, Yokohama 226-8503, Japan

HIGHLIGHTS

- All-solid-state lithium-sulfur batteries are constructed.
- Composite sulfur/carbon electrodes and the thio-LISICON solid electrolyte are used.
- Three-dimensional highly ordered mesoporous carbon is used as a framework.
- This electrode structure provides a highly reversible reaction.
- Higher battery capacity is achieved by decreasing the pore size of the framework.

ARTICLE INFO

Article history:
Received 7 July 2016
Received in revised form
24 August 2016
Accepted 3 September 2016

Keywords:
All-solid-state battery
Lithium–sulfur battery
Carbon matrix
Mesoporous carbon

ABSTRACT

Although the characteristics of lithium–sulfur batteries are advantageous for various applications, batteries with liquid electrolytes show capacity fading due to the dissolution of polysulfides. All-solid-state lithium–sulfur batteries with highly reversible characteristics are developed using a three-dimensional carbon matrix framework structure for the sulfur cathode. Sulfur is introduced into a carbon replica framework with a pore size of 8–100 nm. The composite electrode structure provides high electronic conduction and allows high cathode utilization during the battery reaction. The capacity of cells using a LiAl alloy as the negative electrode and the thio-LISICON (lithium superionic conductor) electrolyte increases when the pore size of the carbon replica is decreased from 100 nm to less than 15 nm. The highest capacity is obtained for the carbon replica with a pore size of 8.6 nm and a wall thickness of 4.7 nm. An examination of the relationship between the charge–discharge capacity and the structure of carbon replicas with different pore sizes and wall thicknesses indicates that three-dimensional highly ordered mesoporous carbon with a small pore size is a promising electrode structure for lithium–sulfur all-solid-state batteries.

1. Introduction

The lithium–sulfur battery as a power storage device is a promising candidate for both small- and large-size applications, such as portable devices, electric vehicles, and stationary applications. Lithium-based systems have the advantage of a high energy density because they are lightweight with a low electrochemical potential. For lithium systems, the sulfur cathode has a high theoretical capacity of 1672 mAh g^{-1}, which is ten times higher than that of the conventional electrode material, $LiCoO_2$. The electrochemical reaction of sulfur with lithium is described by the following formula: $S+2Li^{+}+2e^{-} \rightleftharpoons Li_2S$. Owing to the abundant sources of elemental sulfur and lithium, the lithium/sulfur redox couple might be a promising candidate for safe, inexpensive, and high-capacity batteries. However, lithium–sulfur batteries with a

* Corresponding author. Department of Chemical Science and Engineering, School of Materials and Chemical Technology, Tokyo Institute of Technology, Yokohama 226-8502, Japan.
E-mail address: kanno@echem.titech.ac.jp (R. Kanno).

http://dx.doi.org/10.1016/j.jpowsour.2016.09.009
0378-7753/

liquid electrolyte show significant fading of the charge–discharge capacity owing to the dissolution of polysulfides formed during the battery reaction [1,2]. All-solid-state batteries using sulfide solid electrolytes are more advantageous than batteries with liquid electrolytes because solid–solid contact eliminates the polysulfide dissolution problem. Moreover, the non-flammable characteristic of the solid electrolyte is also an advantage, resulting in extremely high reliability and safety. Furthermore, the all-solid-state configuration has the potential to provide batteries with high power densities [3]. However, the low electronic conductivity of sulfur (5×10^{-30} S cm^{-1} at room temperature) [4] causes rather low utilization of the sulfur electrode in the battery reaction [5,6]. In the present study, we examined a three-dimensional framework electrode structure to improve electronic conduction in composite sulfur cathodes.

Mesoporous carbon has meso-size pores in a carbon matrix [7–10] with ordered arrangements, either in two-dimensions (e.g., CMK-3) or three-dimensions (carbon replica). The carbon replica is synthesized from a template of silica spheres [11] with micro-to nanometer sizes, a uniform size distribution [11–13], and a cubic close packing structure [11,12,14]. The size of the silica spheres can be finely tuned by varying the amount of amino acid in the template [14,15], and thus the size of the pores in the carbon replica (well-ordered mesoporous carbon) can be easily controlled [14,16]. Such ordered mesoporous structures might provide a new electrode framework and allow high electronic conduction in the electrode matrix for all-solid-state batteries.

Previously, we reported that the electrode structure of a sulfur/mesoporous carbon (CMK-3) composite provides highly reversible characteristics to all-solid-state lithium–sulfur batteries. However, the two-dimensional carbon rod structure of CMK-3 provides a fixed pore size in the electrode framework, and the resulting electrode matrix has a large carbon ratio, which reduces the total capacity for practical cells [17]. A new electrode structure that allows for much closer electrode/electrolyte contact might improve electronic conduction and thus the charge–discharge characteristics. Thus, we have optimized the pore size of the electrode framework structure of mesoporous carbon using a carbon replica.

In the present study, the electrode structure was examined to improve the characteristics of lithium–sulfur batteries with thio-LISICON (lithium superionic conductor) [18,19] as a solid electrolyte. Composite electrodes of sulfur and carbon replicas with various pore sizes were fabricated using a gas-phase mixing method. The composite electrode structure improved the utilization of sulfur in the charge–discharge reaction and thus provided a high energy density for all-solid-state lithium–sulfur batteries.

2. Experimental

2.1. Synthesis of carbon replicas and carbon–sulfur composites

Silica nanospheres with uniform sizes of 8–100 nm were synthesized from tetraethyl orthosilicate and L-arginine [11,16]. Varying the size of the silica nanospheres allowed the pore size in the carbon replicas to be controlled [11,14]. Spheres of 8, 12, 14, 20, 40, and 100 nm were used as templates, and the corresponding carbon replicas were indexed as CR8, CR12, CR14, CR20, CR40, and CR100, respectively. The synthesis methods for the carbon replica have been described elsewhere [16]. Silica nanospheres, furfuryl alcohol ($C_5H_6O_2$), and oxalic acid were used as the template, carbon source, and acid catalyst, respectively. Polymerization of the nanosphere samples in the presence of furfuryl alcohol and oxalic acid was promoted at 100 °C for 48 h. The sample was then crushed and carbonized at 120 °C for 0.5 h and 800 °C for 1 h under Ar. The above treatment produced a black powder, which was treated with 5% HF aqueous solution to remove the silica template.

Sulfur–carbon composites were prepared using a previously reported gas-phase mixing method [20]. Sulfur (Kojundo Chemical Laboratory, >99.99% purity) and the carbon replica in a ratio of 30:70 (wt%) were mixed in an argon-filled glove box, sealed in a quartz tube under a vacuum atmosphere, and then heated at 300 °C for 2 h. After heating, the tube was slowly cooled to 20–30 °C.

2.2. Cell fabrication

The test cell was composed of a polyethylene terephthalate cylinder with an inner diameter of 10 mm. A material in the thio-LISICON family, $Li_{3.25}Ge_{0.25}P_{0.75}S_4$, was synthesized using a solid-state reaction for use as the solid electrolyte [18]. The positive electrode was constructed from the sulfur–carbon replica composite and the solid electrolyte, which were mixed in a ball mill (Fritsch P-7 planetary ball milling apparatus) at a ratio of 50:50 (wt %). The solid electrolyte (~70 mg) was pressed into a pellet. The positive electrode powder (5 mg) was dispersed on one side of the electrolyte pellet, and then aluminum mesh with a diameter of 9 mm and a thickness of 0.1 mm as current collector was placed on the cathode powder. The cathode powder and current collector were pressed together at a pressure of 500 MPa using a uniaxial press machine (Riken Kiki Co., Ltd., P–6). A lithium–aluminum composite, consisting of aluminum foil (0.1 mm thickness) and lithium foil (0.1 mm thickness) with a diameter of 10 mm, was used as the negative electrode [21]. The Li/Al ratio is about 38:68 (mol%), which provides a redox potential of 0.38 V (*vs.* Li/Li$^+$). The aluminum foil was attached to the solid electrolyte at a pressure of 500 MPa [21], and the lithium sheet was then attached to the aluminum foil. Copper mesh with a diameter of 9 mm and a thickness of 0.1 mm was placed on the lithium sheet as a current collector, followed by pressing at 8 MPa. The preparation and fabrication of the cells was carried out in a dry argon-filled glove box (H_2O < 0.1 ppm, Miwa MFG Co., Ltd.).

2.3. Characterization methods

The electrochemical properties of the cells were characterized using a multi-channel galvanostat (TOSCAT-3100). Constant currents in the range of 0.013–1.3 mA cm^{-2} were applied to the cells at 25 °C and the cut off voltages for discharging and charging were 0.5 and 3.0 V, respectively. The electrodes were characterized by small angle X-ray scattering measurements using a Rigaku Ultima-IV diffractometer with Cu Kα radiation. The weight ratio of sulfur and carbon in the composite electrode was measured using thermogravimetry (TG). The TG measurements were conducted from 20–30 °C–600 °C at a heating rate of 10 °C min^{-1} under a helium atmosphere. The morphologies of the composite electrodes were investigated using a field emission scanning electron microscope (FE-SEM, Hitachi S-5200) with an acceleration energy of 30.0 kV. The porosity of the cathode composite with open pores was measured using the Brunauer–Emmett–Teller (BET) method with nitrogen gas (Bellsorp-mini). The pore distribution of carbon was calculated using the Barrett–Joyner–Halenda (BJH) method [22].

3. Results and discussion

3.1. Synthesis of carbon replicas and sulfur composites

The advantage of a carbon replica for application as an electrode matrix is its three-dimensional nanopore structure that can accept sulfur and provide electronic conduction to the sulfur cathode complex. The pore size of the carbon replica is easily controlled by

changing the size of the silica template, and the size dependence of the electrode characteristics can be easily examined. SiO_2 spheres with various diameters (8, 12, 14, 20, 40, and 100 nm) are used as templates for carbon replicas (CR8, CR12, CR14, CR20, CR40, and CR100, respectively). The nanosphere samples are polymerized in the presence of furfuryl alcohol and oxalic acid to obtain the carbon replicas, following removal of the silica template. The carbon replicas are then used to prepare sulfur–carbon composites using a gas-phase mixing method.

3.2. SEM characterization of carbon replicas and sulfur composites

Fig. 1 shows FE-SEM photographs of the carbon replicas and the composite electrodes of the carbon replicas with sulfur. The distribution of the pores in each carbon replica is quite uniform with close-packed and spherical pores, resulting in the formation of highly ordered porous carbon frameworks. The spherical pores are three-dimensionally connected through small holes. There is no clear change in the shape of the mesopores after mixing with sulfur. In addition, no aggregate of deposited sulfur is observed in any sample, which indicates that the deposited sulfur is highly distributed on the surface of the carbon replicas. The pore sizes observed for these carbon replicas are 9.2, 42.8, and 107.9 nm for CR12, CR40, and CR100, respectively, which is consistent with those estimated from the size of the SiO_2 templates.

3.3. Adsorption–desorption isotherms

Fig. 2 shows the nitrogen adsorption–desorption isotherms of carbon replicas with pore sizes between 10 and 100 nm, and the composites of these carbon matrixes with sulfur. All of the samples have a type IV isotherm, which is characteristic of a sharp capillary condensation step.

Changing the pore size from 12 to 100 nm shifts the relative pressure (p/p_0) of the main step to higher values (from 0.6 to 0.95), which corresponds to an increase in the adsorption volume. CR100 shows two capillary condensation steps at relative pressures of approximately 0.6 and 0.95, indicating the existence of two kinds of pore with different sizes in the matrix. On mixing sulfur with the carbon replicas, the adsorption volume decreases compared with that of the carbon replica alone, for example, from 450 to 230 cm^3 (STP) g^{-1} and from 1400 to 1200 cm^3 (STP) g^{-1} for CR12 and CR40, respectively. This result indicates that the sulfur introduced by gas-phase mixing is inserted into the pores and attached to the surfaces of the mesopores, thereby decreasing the surface area per unit mass. Fig. 3 shows BJH plots calculated from the nitrogen adsorption isotherms of CR12, CR40, and CR100 and the corresponding composites with sulfur. The peak positions in these plots indicate the pore radii in the carbon replicas. CR12 and CR40 have uniform pore sizes of 8.6 and 42.2 nm, respectively, which decrease slightly to 8.4 and 40.2 nm, respectively, with sulfur mixing. These small changes in the pore size indicate that a uniform thin layer of sulfur is deposited on the mesopore walls.

In the case of CR100, a sharp peak at 59 nm indicates the formation of uniform pores with a diameter of 117.2 nm. However, additional small peaks are observed with pore radii of 5 and 12 nm. These peaks indicate the existence of additional small pores in the carbon matrix, which might be located in gaps between the carbon walls of the ball-shaped pores [12]. After sulfur mixing, no size reduction is observed for the large pore. On the other hand, the pores with 5 and 12 nm radii disappear and show a reduction in size, respectively. This result indicates that sulfur is preferentially deposited in the small pores, while no significant amount of sulfur is deposited on the large pore walls.

Table 1 summarizes the surface area of the mesopores, the average pore diameter, and the total amount of N_2 gas adsorbed by the carbon replicas before and after sulfur mixing. All the carbon replicas have surface areas in the range of 500–600 m^2 g^{-1}. The surface areas of the carbon replicas decrease after sulfur mixing, with particularly large decreases observed for CR12 and CR100. The total amount of N_2 gas adsorbed also decreases after sulfur mixing. However, S/CR40 and S/CR100 maintain V_a values over 1000 cm^3 (STP) g^{-1}, indicating that there are large vacant spaces in their matrixes.

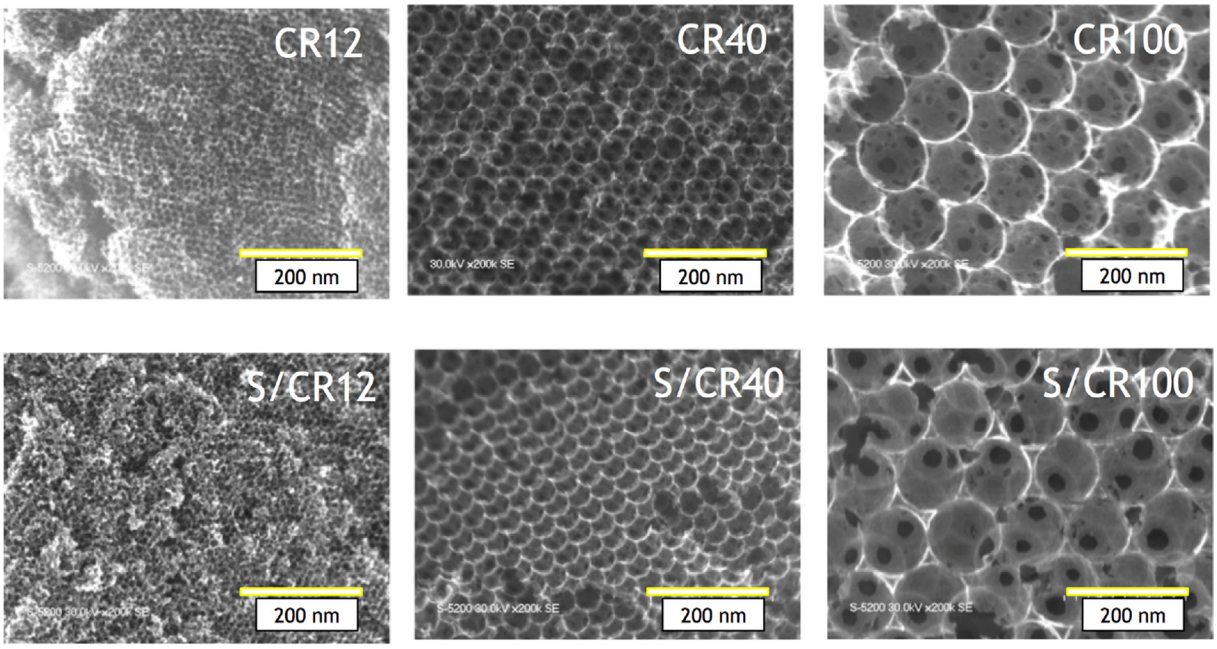

Fig. 1. FE-SEM images of carbon replicas with various pore sizes (CR12, CR40, and CR100, top) and the corresponding sulfur/carbon replica composite materials (bottom).

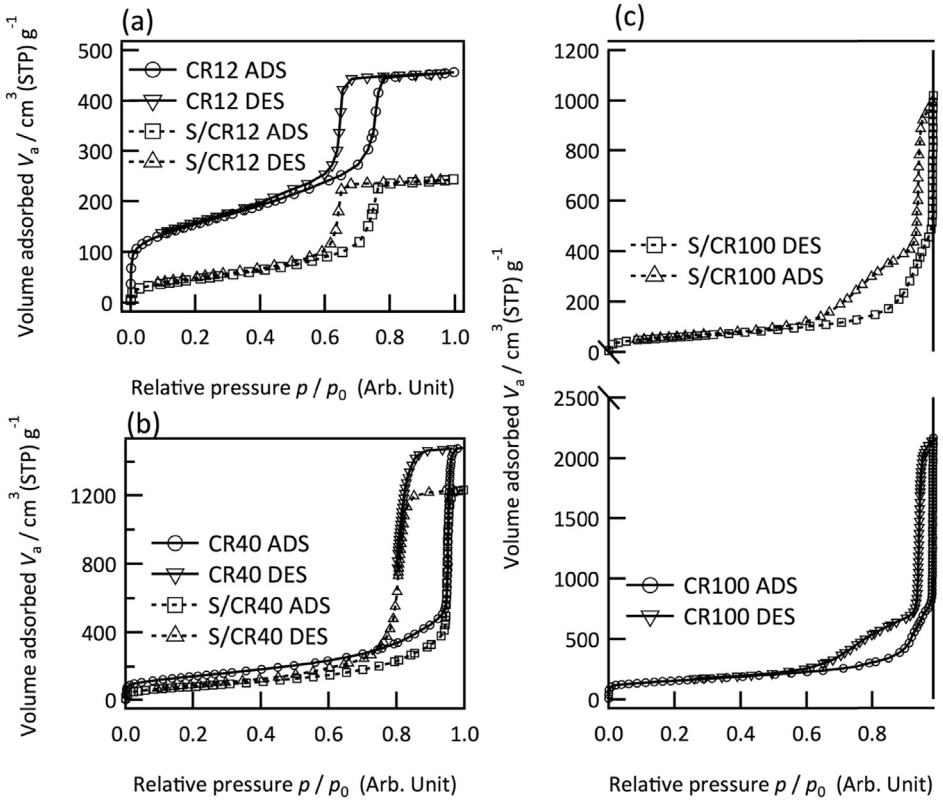

Fig. 2. N_2 adsorption–desorption isotherms of the carbon replicas and corresponding sulfur composite materials: (a) CR12, (b) CR40, and (c) CR100.

3.4. Charge–discharge characteristics of carbon replicas and sulfur composites

Fig. 4(a) shows the first discharge curves of the cells composed of composite electrodes with sulfur and carbon replicas CR12, CR40, and CR100 at a current density of 0.13 mA cm^{-2}. The charge–discharge capacities were calculated based on the nominal sulfur content (30 wt%) in the composite, as the TG analysis revealed that the mean sulfur content in the sulfur/carbon replica composites is 26.5 wt%. The S/CR12 composite electrode has a discharge capacity of 1864 mAh g_{sulfur}^{-1}, which exceeds the theoretical capacity of sulfur, indicating that the carbon matrix may contribute to the battery reaction, in addition to decomposition of the solid electrolyte at low voltages [17,23]. Taking into account the total weight of sulfur and carbon, the discharge capacity is calculated as 559 mAh g_{total}^{-1}. The discharge capacities of the S/CR40 and S/CR100 composite electrodes are 880 and 210 mAh g_{sulfur}^{-1}, respectively. This behavior reveals that a smaller pore size improves the electrochemical performance of the sulfur/carbon replica batteries. Based on the BET analysis, these S/CR composites have similar surface areas (170–310 m^2 g^{-1}). Therefore, relatively large vacant spaces in the matrix could suppress the electrochemical capacity of batteries that employ carbon replicas with large pore sizes, as the vacant space cannot contribute to ionic/electronic conduction. Notably, S/CR40 and S/CR100 show relatively large volumes adsorbed compared with that of S/CR12. In addition, the lower capacity of S/CR100 might be due to the introduction of sulfur into the small pores, where it cannot easily contribute to the battery reaction. As shown in Fig. 1(b), the IR drops at the beginning of discharge also indicate that sulfur/carbon replica composites with smaller pore sizes exhibit improved behavior, as the cell voltage of the battery drops to 2.3, 1.8, and 1.6 V for S/CR12, S/CR40, and S/CR100, respectively.

The curves exhibit only one plateau, similar to that previously observed for sulfur/CMK-3 electrodes in a solid-state battery system [17]. Moreover, the cell voltages of the composite electrode batteries are slightly lower than those of conventional Li/S batteries, which also suggests that there is an interaction between lithium and the sulfur/carbon composite matrix.

Fig. 4(c) shows the discharge capacity during cycling of the S/CR composite materials at a current density of 0.065 mA cm^{-2}. S/CR40 and S/CR100 show a significant decrease of capacity below 280 mAh g_{sulfur}^{-1} in the initial few cycles, while S/CR12 maintains a capacity of over 500 mAh g_{sulfur}^{-1}, even after 10 cycles. At the 20th cycle, S/CR12, S/CR40, and S/CR100 have discharge capacities of approximately 366, 126, and 57 mAh g_{sulfur}^{-1}, respectively. The smaller pore size of the carbon matrix provides a larger discharge capacity after the cycling trial, which indicates that the cycle capability may be improved by regulating the pore size of the carbon replica. Fig. 4(d) shows the relationship between the initial discharge capacity and the current density for the sulfur/carbon replica composites. The discharge capacity decreases with increasing current density for all of the composite electrodes. However, a relatively high capacity is maintained for S/CR12 at any current density, and the capacity is comparable to that of the S/CMK-3 composite cathode [17]. S/CR12 maintains the highest capacity of 489 mAh g_{sulfur}^{-1}, even with a current density of 1.3 mA cm^{-2}, while S/CR40 and S/CR100 have small capacities of less than 180 mAh g_{sulfur}^{-1}. These results are clear evidence that decreasing the pore size contributes to an increase of the rate capability of these batteries. The best electrochemical performance for the cathodes is achieved with an optimal pore size of approximately 9 nm.

To examine other factors that could affect the battery

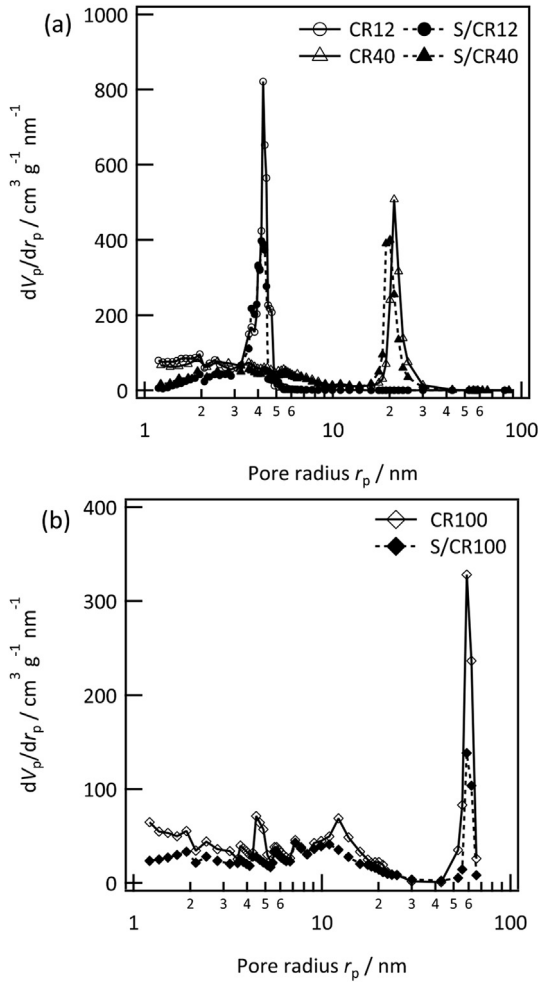

Fig. 3. Mesopore size distributions for the carbon replicas and corresponding sulfur composite materials: (a) CR12 and CR40, and (b) CR100.

performance, various carbon replicas with comparable pore sizes (<25 nm) were prepared. Table 2 summarizes the pore sizes and specific surface areas of CR8, CR12, and CR20, along with the discharge capacity of the corresponding sulfur/carbon replica composites. BJH plots for these samples confirm comparable pore sizes of 6–11 nm. However, the first discharge capacities and specific surface areas of these samples are clearly different (Table 2). These values indicate that for comparable mesopore sizes, a carbon replica with a smaller surface area provides a higher capacity. The smaller surface area per unit mass of the carbon replica could be attributed to the thicker carbon wall between the mesopores in the structure. Generally, a large surface area is suitable for accommodating sulfur at the surface, which could contribute to a large lithium storage capacity. However, the higher capacity obtained for the composite with a smaller surface area indicates that the carbon wall might also be an important parameter for lithium storage.

3.5. Characterization using small angle X-ray scattering and X-ray diffraction

Small angle X-ray scattering is an efficient technique for characterizing the structure of the mesopores and the surface of the carbon matrix before and after sulfur mixing. Small angle X-ray scattering measurements were obtained for all of the carbon replicas and corresponding sulfur composites. Fig. 5 shows representative small angle X-ray profiles and X-ray diffractions of CR12 and S/CR12. The observation of several peaks around $Q = 0.06$ and 0.1 $Å^{-1}$ indicates ordered mesopores in the carbon replica with a uniform pore size, as observed by SEM. This result is also consistent with the sharp peaks observed in the BJH plot. The peak at $Q = 0.058$ $Å^{-1}$ for CR12 corresponds to the 111 reflection of the ordered pore with cubic close packing. The interplanar spacing, d_{111}, is found to be 10.83 nm. As the pore size estimated from the BJH plot is 8.6 nm, the thickness of the carbon wall between pores is calculated to be 4.7 nm. However, the thickness of the carbon wall for CR20 is 4.0 nm, which is thinner than that of CR12. As the composite electrodes with thicker walls in the carbon replica have larger discharge capacities, the wall thickness might affect the battery performance.

After gas phase mixing of sulfur with the carbon replica, no changes in the peak positions for the mesopores are observed. This result indicates that the distance between scatterers is the same after sulfur mixing. Although sulfur is coated on the surfaces of the mesopores, no changes are observed in the spherical form of the pore or the distance between pore centers. Thus, the carbon replicas still have uniformly ordered pores after sulfur mixing.

The small angle X-ray and X-ray diffraction patterns at $Q = 0.2519–3.991$ $Å^{-1}$ were analyzed to determine the interplanar spacing of carbon (h0) and (00l) and roughness of the surface using the following equation.

$$I = AQ^p + B_1\exp\{-(Q - Q_1)^2/\sigma_1^2\} + B_2\exp\{-(Q - Q_1/2)^2/\sigma_2^2\} + B_3\exp\{-(Q - Q_3)^2/\sigma_3^2\} + Bkg$$

The first term on the right-hand side of this equation gives Porod low when $p = -4$, corresponding to a scatterer with a smooth flat surface. Moreover, the fractal dimension (D_s) of the surface is given by $D_s = 6 + p$. The second to fourth terms are the Gaussian functions corresponding to the 002, 001, and 10 Bragg peaks, respectively. Table 3 shows D_s, the distance between graphene layers (d_{002}), and information about the in-plane structure (d_{10}), which are calculated from p, Q_1, and Q_3, respectively. Taking into account that the dominant surface area is assigned to mesopores, the observed changes in the D_s values reveal that sulfur is deposited on the carbon surface in the pores. The calculated values of D_s for CR12 decrease from 3 to 2.6 after sulfur mixing, and similar tendencies are confirmed for CR8 and CR20. This result indicates that the complexity of the mesopore surface decreases with sulfur

Table 1
Mesopore surface area, average pore diameter, and total amount of N_2 gas adsorbed for carbon replicas before and after sulfur mixing.

		CR12	CR40	CR100
Mesopore surface area S/m^2 g^{-1}	CR	549	593	545
	S/CR	171	305	214
Pore diameter d/nm	CR	8.6	42.2	117.2
	S/CR	8.4	40.2	117.2
Volume adsorbed V_a at $p/p_0 \approx 1$/cm^3 (STP) g^{-1}	CR	456	1483	2164
	S/CR	244	1232	1019

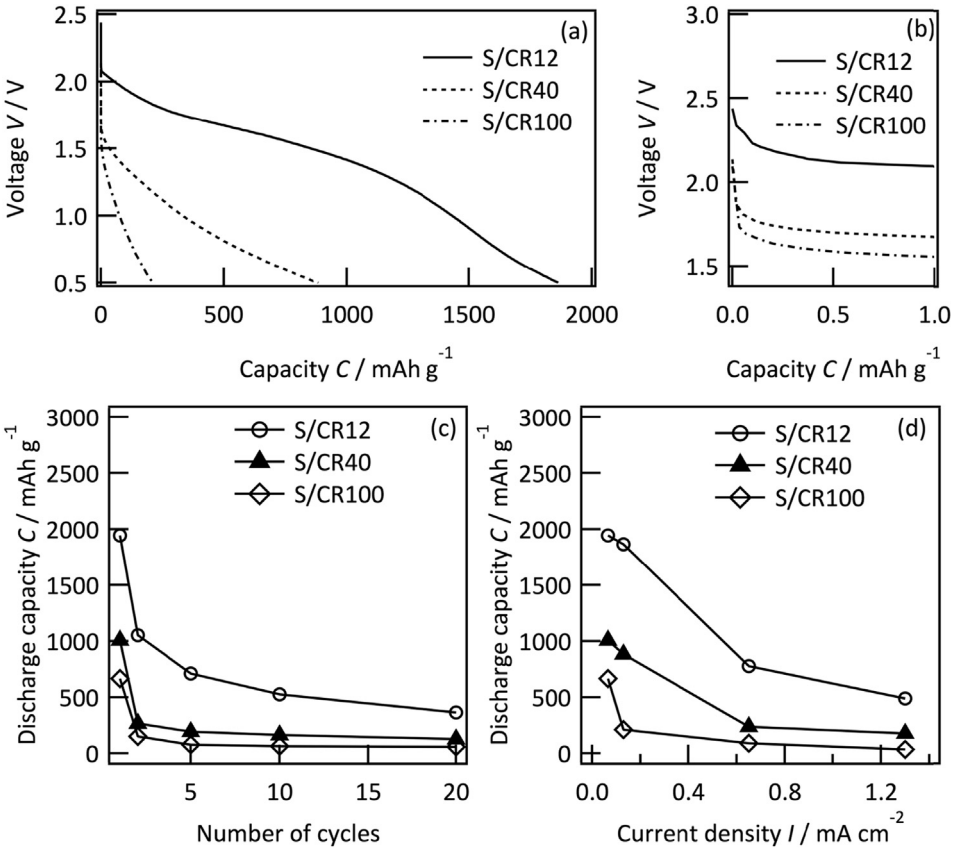

Fig. 4. (a) First discharge curves, (b) expanded view of the first discharge curves at low capacities, (c) cycle characteristics, and (d) rate characteristics of the all-solid-state batteries using composite electrodes of S/CR12, S/CR40, and S/CR100.

Table 2
Correlation of pore size, first discharge capacity, and specific surface area for CR8, CR12, and CR20.

	Pore size d/nm	Surface area S/m^2 g^{-1}	First discharge capacity C/mAh g$^{-1}_{sulfur}$
CR8	6.5	2010	906
CR12	8.6	549	1944
CR20	10.6	1010	1282

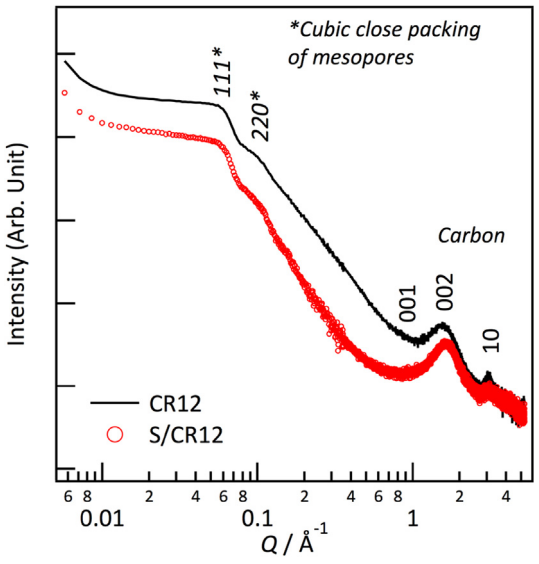

Fig. 5. Small angle X-ray scattering profiles for CR12 and S/CR12.

Table 3
Fractal dimensions of the pore surface (D_s), distance between graphene layers (d_{002}), and information about in-plane structure (d_{10}) for carbon replicas and corresponding sulfur composites.

	CR12	S/CR12	CR14	S/CR14	CR20	S/CR20
D_s	3	2.6	3	2.6	3	2.4
d_{002}/Å	3.83	3.95	3.81	3.74	3.88	3.74
d_{10}/Å	2.01	2.03	2.05	2.03	2.05	2.05

mixing. No significant relation between the surface roughness of sulfur on the wall and battery performance has been confirmed.

The d_{002} value of CR12 increases from 3.83 to 3.95 Å with a decrease in the 001 diffraction intensity, which indicates a decrease in the AAAA stacking symmetry with sulfur mixing. However, no changes are observed for the in-plane structure of d_{10}. For CR14 and CR20, the d_{002} value decreases with no change in d_{10} with sulfur mixing. These results indicate that the sulfur deposited on the carbon wall interacts with the edge of the graphene layer to change the interplanar space of (00l). The sulfur interacting with carbon reacts with lithium, and the reaction of sulfur with carbon might

affect the deposition of lithium on the carbon wall, resulting in a capacity value at the first discharge that is larger than the theoretical capacity of sulfur. The changes in the cell potential also suggest an interaction between carbon and sulfur on the surface. The wall thickness effects and 00*l* interplanar changes indicate that the carbon wall could play a key role in the battery reaction when using S/CR composite electrodes. As the first discharge capacity of S/CR12 (1944 mAh g^{-1}) exceeds that of the S/CMK-3 composite (1600 mAh g^{-1}) [17], the optimum pore size and carbon wall thickness are about 9 and 5 nm, respectively, for the carbon replica as a conductive framework. These optimal values could be related to two factors: (i) the small pore size can contribute to reducing the vacant space in the matrix, and (ii) the thick carbon wall can provide a stable framework as a carbon matrix and reaction field for carbon and sulfur during the mixing process.

4. Conclusions

All-solid-state lithium–sulfur batteries were examined using composite electrodes of sulfur and carbon replicas with three-dimensional mesoporous structures. The structures of the sulfur–carbon composites were determined by BET measurements and X-ray scattering techniques. The all-solid-state cells with the thio-LISICON electrolyte and LiAl negative electrode have high discharge capacity and high charge–discharge reversibility. The capacity increased when the size of the mesopores decreased from 100 nm to less than 15 nm. At a comparable pore size of 10 nm, the capacity further increased with the thickness of the carbon wall, with the highest discharge capacity obtained for CR12 with a 4.7 nm thick carbon wall. Sulfur mixed with the carbon replicas was found to exist on the carbon surface of the pores and may be inserted into the carbon wall through the edges of the graphene layer. The sulfur at these positions contributed to the charge–discharge reaction. Thus, three-dimensional highly ordered mesoporous carbon with a small pore size is a promising electrode structure that provides high electronic conductivity and high sulfur utilization for the charge–discharge reaction of lithium–sulfur all-solid-state batteries.

Acknowledgements

This work was partly supported by a Grant-in-Aid from the Advanced Low Carbon Technology Research and Development Program, Specially Promoted Research for Innovative Next Generation Batteries (ALCA-SPRING) of the Japan Science and Technology Agency (JST).

References

[1] R.D. Rauh, K.M. Abraham, G.F. Pearson, J.K. Surprenant, S.B. Brummer, A lithium/dissolved sulfur battery with an organic electrolyte, J. Electrochem. Soc. 126 (1979) 523–527.
[2] J. Shim, K.A. Striebel, E.J. Cairns, The lithium/sulfur rechargeable cell: effects of electrode composition and solvent on cell performance, J. Electrochem. Soc. 149 (2002) A1321–A1325.
[3] Y. Kato, S. Hori, T. Saito, K. Suzuki, M. Hirayama, A. Mitsui, M. Yonemura, H. Iba, R. Kanno, High-power all-solid-state batteries using sulfide superionic conductors, Nat. Energy 1 (2016) 16030.
[4] J.A. Dean, Lange's Handbook of Chemistry, McGraw-Hill, New York, 1985.
[5] D. Marmorstein, T.H. Yu, K.A. Striebel, F.R. McLarnon, J. Hou, E.J. Cairns, Electrochemical performance of lithium/sulfur cells with three different polymer electrolytes, J. Power Sources 89 (2000) 219–226.
[6] H. Yamin, E. Peled, Electrochemistry of a nonaqueous lithium/sulfur cell, J. Power Sources 9 (1983) 281–287.
[7] L. Wang, S. Lin, K. Lin, C. Yin, D. Liang, Y. Di, P. Fan, D. Jiang, F.-S. Xiao, A facile synthesis of highly ordered mesoporous carbon monolith with mechanically stable mesostructure and superior conductivity from SBA-15 powder, Microporous Mesoporous Mater 85 (2005) 136–142.
[8] A.B. Fuertes, S. Alvarez, Graphitic mesoporous carbons synthesised through mesostructured silica templates, Carbon 42 (2004) 3049–3055.
[9] P.M. Barata-Rodrigues, T.J. Mays, G.D. Moggridge, Structured carbon adsorbents from clay, zeolite and mesoporous aluminosilicate templates, Carbon 41 (2003) 2231–2246.
[10] S. Han, M. Kim, T. Hyeon, Direct fabrication of mesoporous carbons using in-situ polymerized silica gel networks as a template, Carbon 41 (2003) 1525–1532.
[11] T. Yokoi, Y. Sakamoto, O. Terasaki, Y. Kubota, T. Okubo, T. Tatsumi, Periodic arrangement of silica nanospheres assisted by amino acids, J. Am. Chem. Soc. 128 (2006) 13664–13665.
[12] J. Tang, X. Zhou, D. Zhao, G.Q. Lu, J. Zou, C. Yu, Hard-sphere packing and icosahedral assembly in the formation of mesoporous materials, J. Am. Chem. Soc. 129 (2007) 9044–9048.
[13] W. Stöber, A. Fink, E. Bohn, Controlled growth of monodisperse silica spheres in the micron size range, J. Colloid Interface Sci. 26 (1968) 62–69.
[14] R. Watanabe, T. Yokoi, E. Kobayashi, Y. Otsuka, A. Shimojima, T. Okubo, T. Tatsumi, Extension of size of monodisperse silica nanospheres and their well-ordered assembly, J. Colloid Interface Sci. 360 (2011) 1–7.
[15] T. Yokoi, M. Iwama, R. Watanabe, Y. Sakamoto, O. Terasaki, Y. Kubota, J.N. Kondo, T. Okubo, T. Tatsumi, Synthesis of well-ordered nanospheres with uniform mesopores assisted by basic amino acids, in: R. Xu, Z. Gao, J. Chen, W. Yan (Eds.), From Zeolites to Porous MOF Materials - the 40th Anniversary of International Zeolite Conference, Proceedings of the 15th International Zeolite Conference, Elsevier, Amsterdam, 2007, pp. 1774–1780.
[16] T. Yokoi, R. Watanabe, S. Ohta, J.N. Kondo, T. Okubo, T. Tatsumi, Preparation of three-dimensionally interconnected ordered mesoporous carbons by using novel silica nanospheres as template, in: A. Sayari, M. Jaroniec (Eds.), Nanoporous Materials: Proceedings of the 5th International Symposium, World Scientific, Singapore, 2008, pp. 275–282.
[17] M. Nagao, Y. Imade, H. Narisawa, T. Kobayashi, R. Watanabe, T. Yokoi, T. Tatsumi, R. Kanno, All-solid-state Li–sulfur batteries with mesoporous electrode and thio-LISICON solid electrolyte, J. Power Sources 222 (2013) 237–242.
[18] R. Kanno, M. Murayama, Lithium ionic conductor thio-LISICON: the Li_2S GeS_2 P_2S_5 system, J. Electrochem. Soc. 148 (2001) A742–A746.
[19] T. Matsumura, K. Nakano, R. Kanno, A. Hirano, N. Imanishi, Y. Takeda, Nickel sulfides as a cathode for all-solid-state ceramic lithium batteries, J. Power Sources 174 (2007) 632–636 (13th International Meeting on Lithium Batteries).
[20] T. Kobayashi, Y. Imade, D. Shishihara, K. Homma, M. Nagao, R. Watanabe, T. Yokoi, A. Yamada, R. Kanno, T. Tatsumi, All solid-state battery with sulfur electrode and thio-LISICON electrolyte, J. Power Sources 182 (2008) 621–625.
[21] R. Kanno, M. Murayama, T. Inada, T. Kobayashi, K. Sakamoto, N. Sonoyama, A. Yamada, S. Kondo, A self-assembled breathing interface for all-solid-state ceramic lithium batteries, Electrochem. Solid-State Lett. 7 (2004) A455–A458.
[22] E.P. Barrett, L.G. Joyner, P.P. Halenda, The determination of pore volume and area distributions in porous substances. I. Computations from nitrogen isotherms, J. Am. Chem. Soc. 73 (1951) 373–380.
[23] M. Sakuma, K. Suzuki, M. Hirayama, R. Kanno, Reactions at the electrode/electrolyte interface of all-solid-state lithium batteries incorporating Li–M (M = Sn, Si) alloy electrodes and sulfide-based solid electrolytes, Solid State Ion. 285 (2016) 101–105.